Science Advances
AAAS

Supplementary Materials for

Nanoscale covalent organic framework-mediated pyroelectrocatalytic activation of immunogenic cell death for potent immunotherapy

Xingguang Li *et al.*

Corresponding author: Xingguang Li, lixingguang@ecust.edu.cn; Pei-Nian Liu, liupn@ecust.edu.cn; Huijing Xiang, xianghuijing@shu.edu.cn

Sci. Adv. **10**, eadr5145 (2024)
DOI: 10.1126/sciadv.adr5145

This PDF file includes:

Supplementary Text

Materials

Chemicals used in this work: ethanol, dichloromethane, *n*-hexane, toluene, and *o*-xylene were purchased from GENERAL-REAGENT (Titan, China). Silica gel (200-300 mesh) and neutral alumina used for column chromatography was purchased from Shanghai Zhonghe Chemical Technology Co., Ltd. Fetal bovine serum (FBS), Dulbecco's Modified Eagle Medium (DMEM), and 0.25% trypsin-ethylene diamine tetraacetic acid (EDTA) solution was purchased from Thermo Fisher Scientific (USA). 2',7'-dichlorodihydrofluorescein diacetate (DCFH-DA) were purchased from Biyotime Biotechnology Co., Ltd. 1,3-Diphenylisobenzofuran (DPBF) and 2,2,6,6-tetramethylpiperidine (TMEP) were obtained from Bidepharm (China). Female BALB/cJGpt mice (Strain NO. N000020) and Female BALB/c-Nude (Strain NO. D000521) were obtained from the GemPharmatech Co., Ltd..

Pyro-current measurements

Pyro-currents were recorded on an electrochemical workstation (Autolab Nova). TPAD-COF NPs (10 mg mL^{-1}) were mixed with ethanol (10 μL) and Nafionper fluorinated resin solution (10 μL), the mixture was spread on a glass electrode, and then immersed in 30 mL of 0.5 M Na_2SO_4 solution. The pyro-current and potential of the solution under alternating NIR laser irradiation (1.0 W cm^{-2}) were monitored.

Cell culture

The mouse breast cancer line (4T1 cells, CSTR:19375.09.3101MOUTCM32) and Human Umbilical Vein Endothelial Cells (HUVEC, 4201PAT-CCTCC02060) was purchased from the Shanghai Institute of Cells, Chinese Academy of Sciences. 4T1 cells and HUVEC were cultured in Roswell Park Memorial Institute (RPMI)-1640 medium (Gibco) containing 10% fetal bovine serum (FBS, Gibco) and 1% penicillin-streptomycin (Invitrogen) at 37°C under 5% CO_2.

In vitro live/dead staining analysis

4T1 cells were cultured overnight in confocal dishes (10^5 cells/dish), and then treated as follows, including PBS, Laser, TPAD-COF NPs, and TPAD-COF NPs + Laser. After washed with PBS, calcein-AM/PI were added to the CLSM dishes of different groups to label live/dead cells, respectively. After staining for 30 min, the cells were rinsed and observed by CLSM.

In vitro cell apoptosis detection

4T1 cells were inoculated into 6-well plates overnight, and then received different treatments, including PBS, Laser, TPAD-COF NPs, TPAD-COF NPs + Laser. After rinsed with PBS, the cells were collected by trypsinization and centrifugation, labeled with Annexin V-FITC and PI, and analyzed by flow cytometry.

In vivo toxicity assay

Female Balb/c mice were randomized into 3 groups (n = 5), including PBS, TPAD-COF NPs (10 mg kg^{-1}), and TPAD-COF NPs (20 mg kg^{-1}), followed by 14 days of feeding. The mouse body weights of each group were monitored every 2 days. Finally, the mice were sacrificed, the blood and major organs of each group were collected for blood examination and histological analysis, respectively.

Immune response analysis

The cell suspensions of tumor tissues in diverse treatment groups were labeled with anti-CD80-PE, anti-CD86-APC, and anti-CD11c-FITC for 30 min at 4°C, and analyzed by flow cytometry for in vivo DC maturation evaluation. After removal of excess antibody by centrifugation, the lymphocyte suspensions were analyzed by flow cytometry. For $CD8^+$ and $CD4^+$ T cell analysis in spleen and tumor tissues, cell suspensions of diverse groups were labeled with anti-CD3-FITC, anti-CD4-APC, and anti-CD8-PE, and then analyzed by flow cytometry and immunofluorescence staining, respectively. In addition, Tregs suspensions were labeled with anti-CD4-APC, anti-Foxp3-PE for flow cytometry analysis. Furthermore, M1 and M2 macrophages were stained with anti-F4/80-PE, anti-CD80-PE and anti-CD206 for flow cytometry analysis. Additionally, the expression levels of cytokines were detected by ELISA kits.

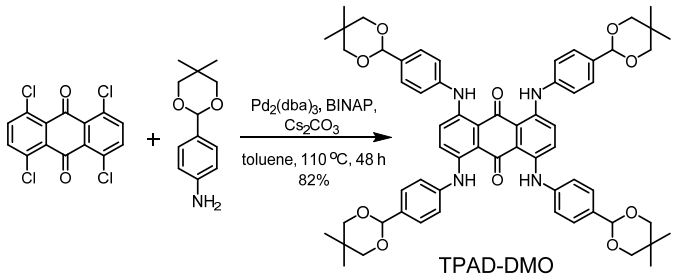

TPAD-DMO

Fig. S1. Synthetic route of 1,4,5,8-tetrakis((4-(5,5-dimethyl-1,3-dioxan-2-yl) ph-enyl) amino) anthracene-9,10-dione (TPAD-DMO).

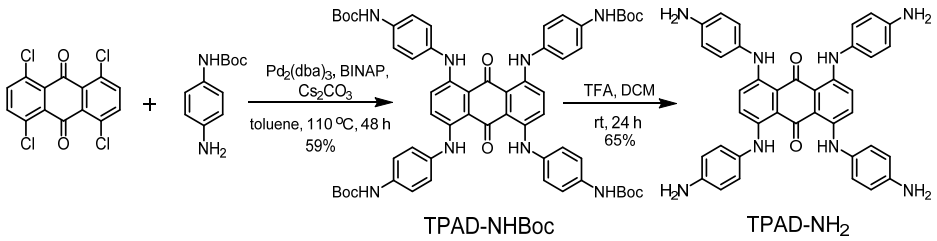

Fig. S2. Synthetic route of 1,4,5,8-tetrakis((4-aminophenyl) amino) anthraxcene-9,10-dione (TPAD-NH_2).

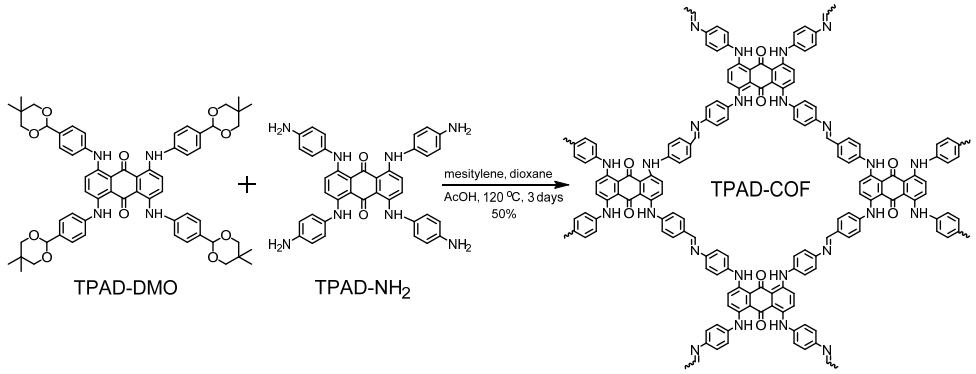

Fig. S3. Synthetic route of TPAD-COF.

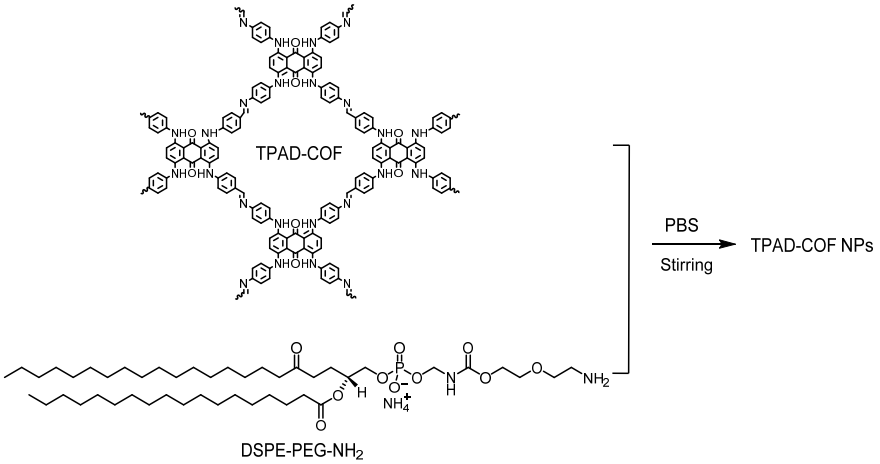

Fig. S4. Synthetic route of TPAD-COF NPs.

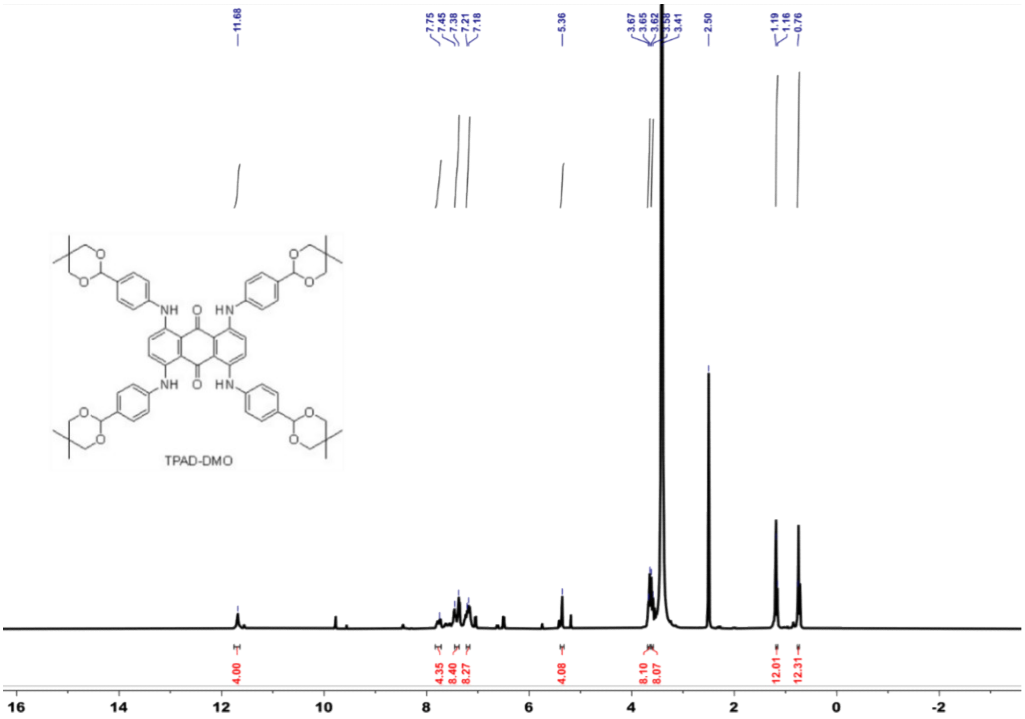

Fig. S5. ^{1}H NMR of TPAD-DMO.
^{1}H NMR (400 MHz, DMSO-d_6) δ 11.68 (s, 4H), 7.75 (s, 4H), 7.41 (d, J = 28.0 Hz, 8H), 7.20 (d, J = 11.8 Hz, 8H), 5.36 (s, 4H), 3.66 (d, J = 10.4 Hz, 8H), 3.60 (d, J = 13.8 Hz, 8H), 1.17 (d, J = 13.2 Hz, 12H), 0.76 (s, 12H).

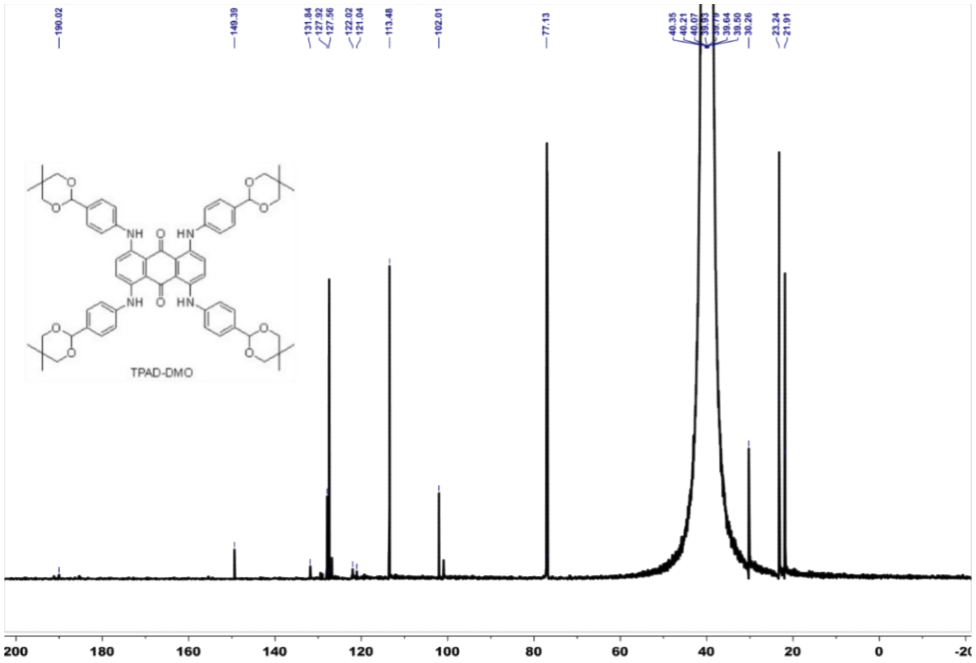

Fig. S6. ^{13}C NMR of TPAD-DMO.
^{13}C NMR (150 MHz, DMSO-d_6) δ 190.0, 149.4, 131.8, 127.9, 127.5, 122.0, 121.0, 113.5, 102.0, 77.1, 30.3, 23.2, 21.9.

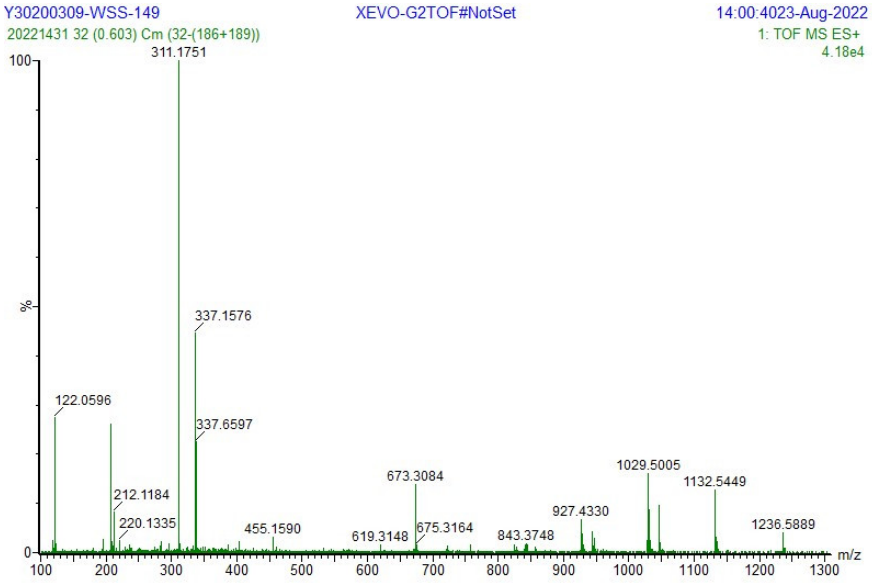

Fig. S7. High-resolution mass spectrum (HRMS, ESI) of TPAD-DMO.
HRMS (ESI): m/z [M + H] $^{+}$ calcd. for $C_{62}H_{69}N_4O_{10}^{+}$: 1029.4856; found: 1029.5005.

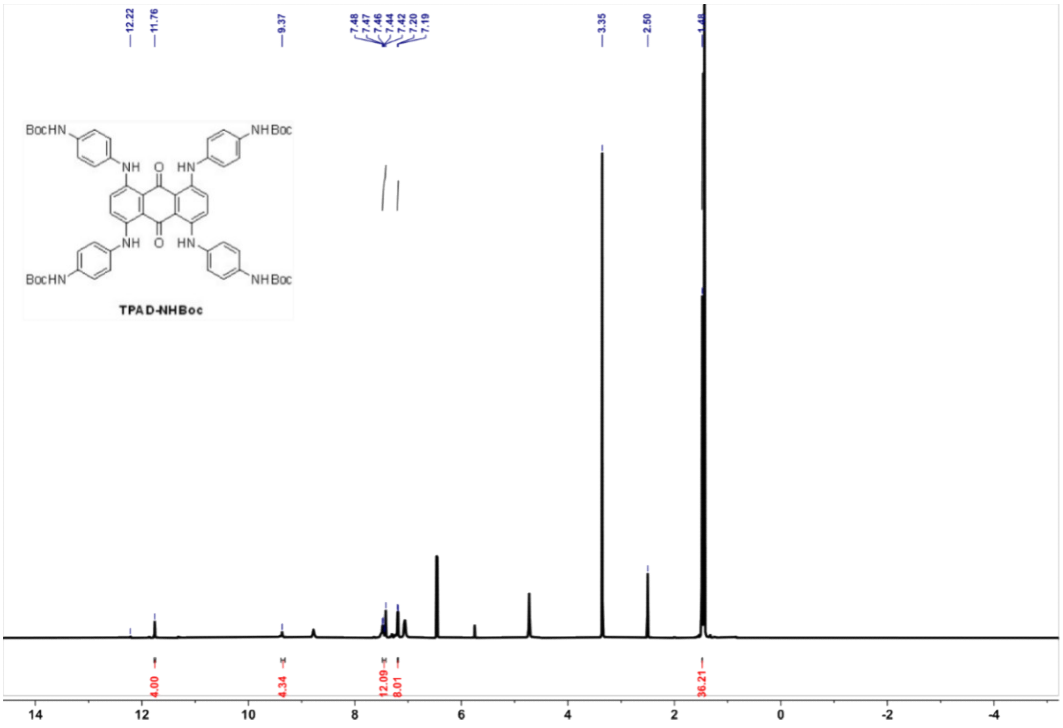

Fig. S8. ^{1}H NMR of TPAD-NHBoc.
^{1}H NMR (400 MHz, DMSO-d_6) δ 11.76 (s, 4H), 9.37 (s, 4H), 7.48-7.42 (m, 12H), 7.19 (d, J = 6.0 Hz, 8H), 1.48 (s, 36H).

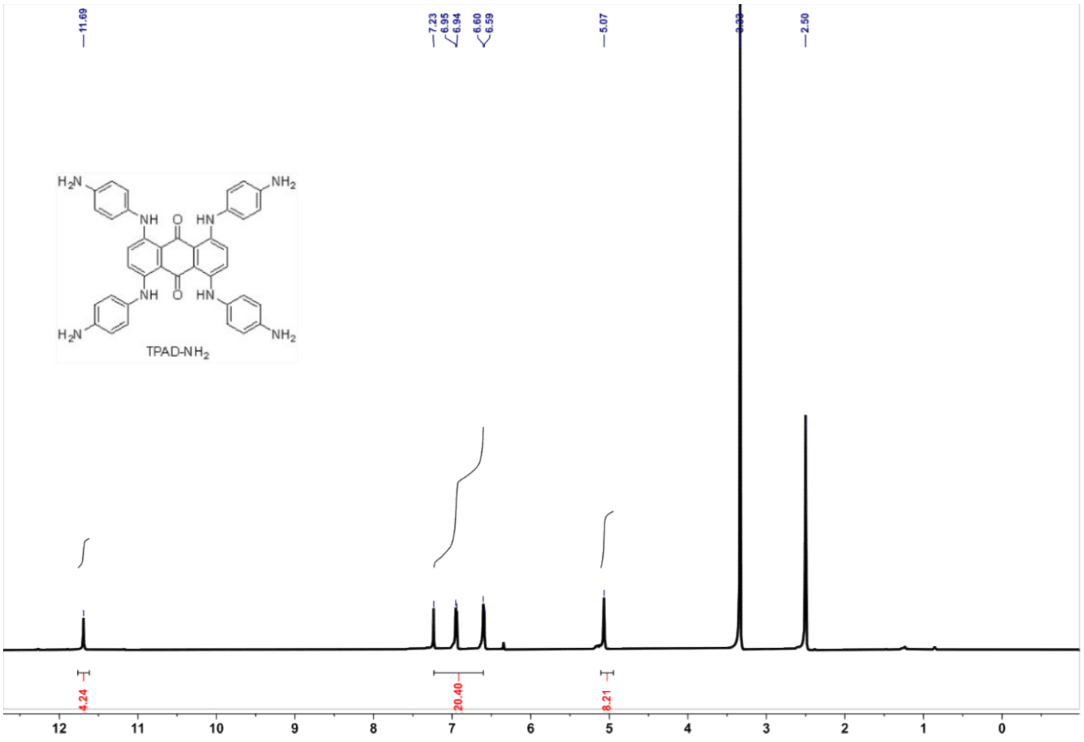

Fig. S9. ^{1}H NMR of TPAD-NH_2.
^{1}H NMR (400 MHz, DMSO-d_6) δ 11.69 (s, 4H), 7.23-6.59 (m, 20H), 5.07 (s, 8H).

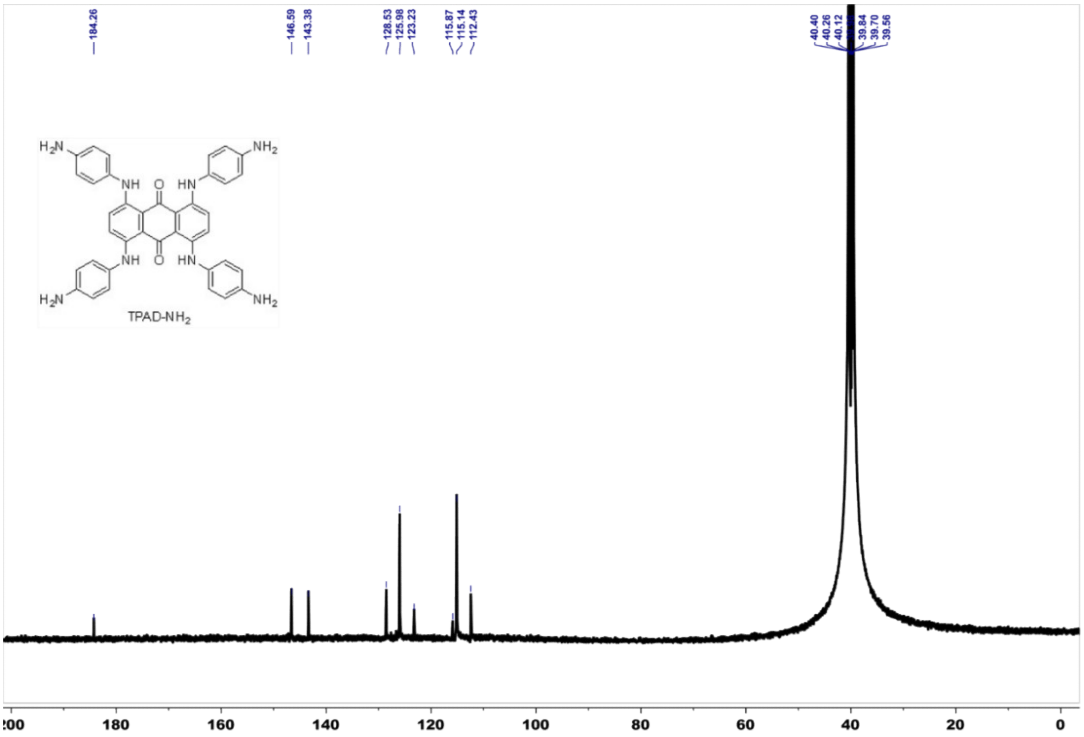

Fig. S10. ^{13}C NMR of TPAD-NH_2.
^{13}C NMR (150 MHz, DMSO-d_6) δ 184.2, 146.5, 143.3, 128.5, 126.0, 123.2, 115.9, 115.1, 112.4.

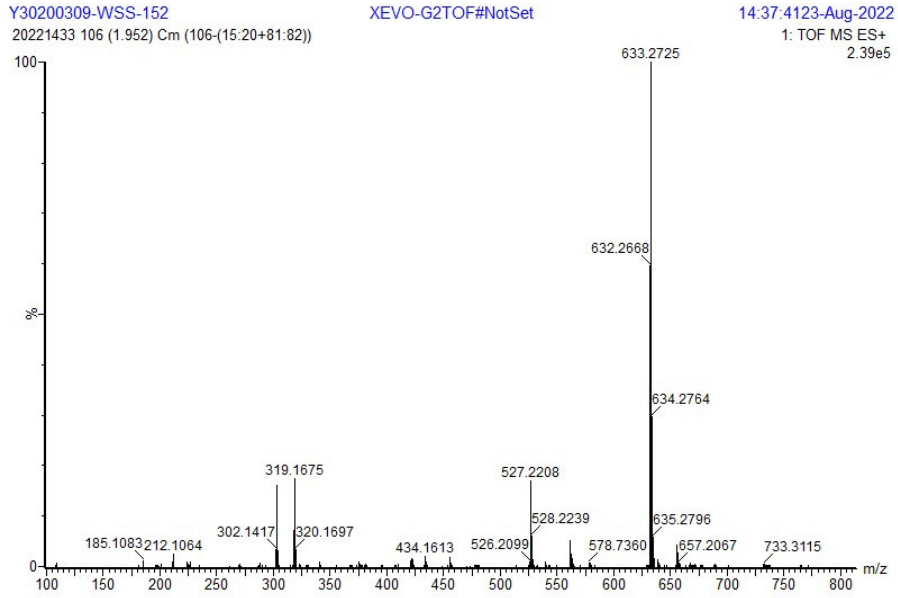

Fig. S11. HRMS (ESI) of TPAD-NH_2.
HRMS (ESI): m/z [M + H] $^+$ calcd. for $C_{38}H_{33}N_8O_2^+$: 633.2569; found: 633.2725.

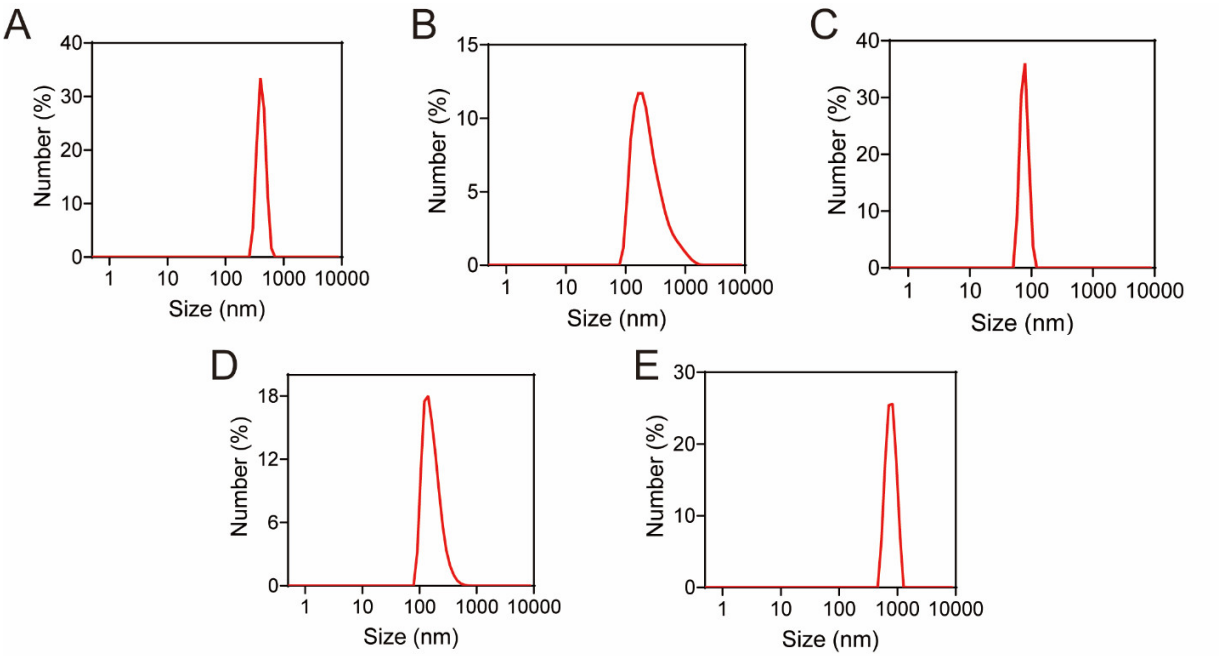

Fig. S12. Size distribution for various concentrations of TPAD-COF NPs, including (**A**) 10 μg mL^{-1}, (**B**) 50 μg mL^{-1}, (**C**) 100 μg mL^{-1}, (**D**) 200 μg mL^{-1}, and (**E**) 500 μg mL^{-1}.

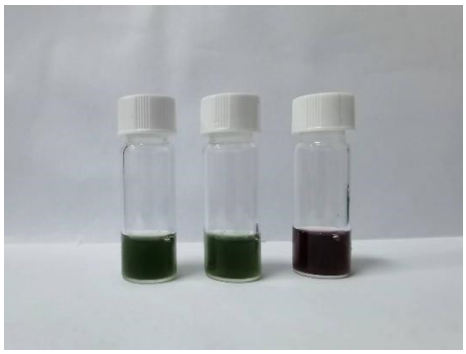

Fig. S13. Photograph of TPAD-COF NPs in PBS, water, and DMEM (from left to right).

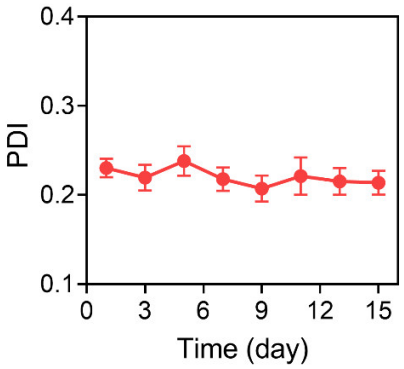

Fig. S14. Polydispersity index (PDI) of TPAD-COF NPs in PBS within 15 days (n = 3).

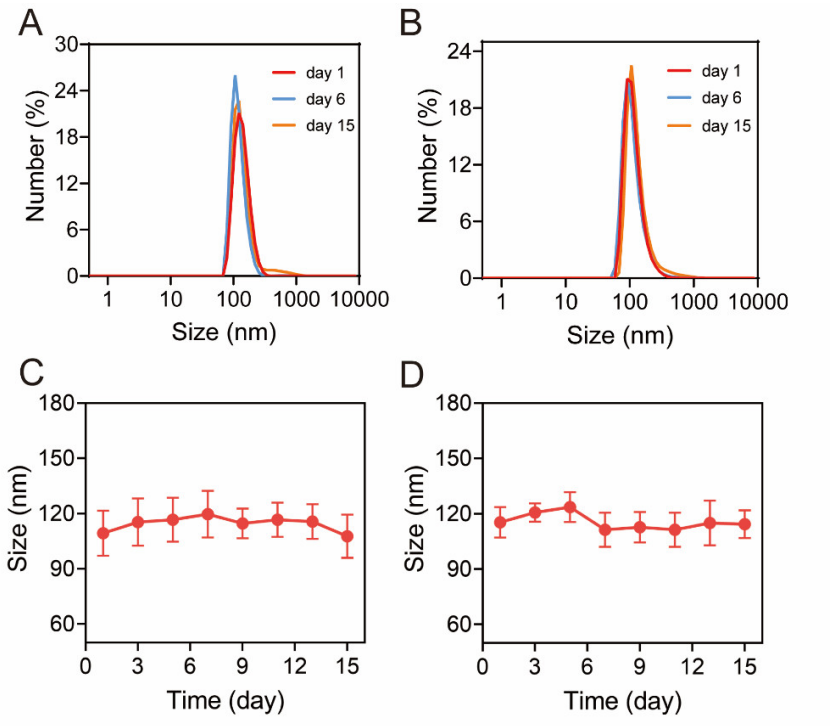

Fig. S15. Dynamic light scattering analysis of TPAD-COF NPs in (**A** and **C**) DMEM, and (**B** and **D**) 10% FBS in water over 15 days (n = 3).

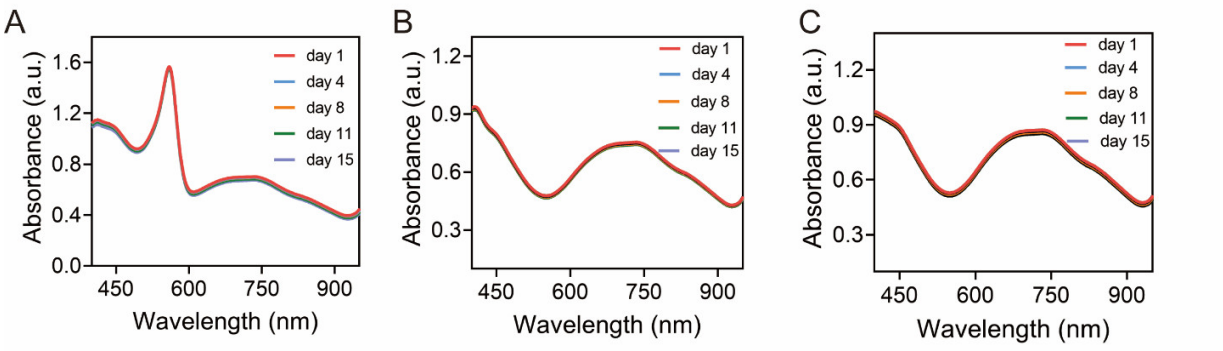

Fig. S16. UV-vis absorption spectra of TPAD-COF NPs in (**A**) DMEM, (**B**) 10% FBS in water, and (**C**) PBS over 15 days.

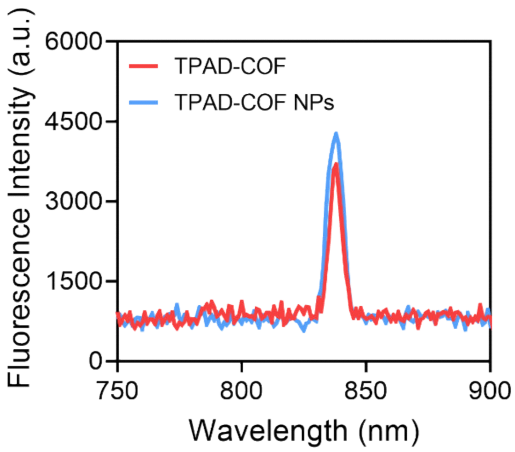

Fig. S17. Fluorescence spectra of TPAD-COF and TPAD-COF NPs.

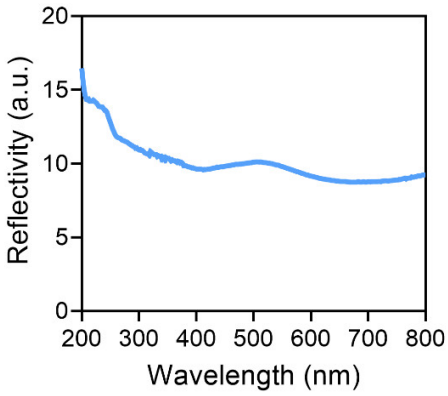

Fig. S18. UV-vis diffuse reflectance spectrum of TPAD-COF NPs.

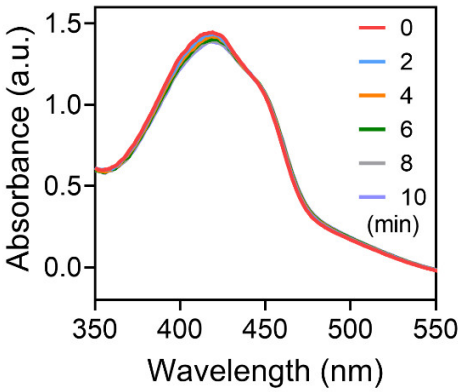

Fig. S19. UV-vis absorption spectra of DPBF containing PBS solution under NIR laser irradiation for 10 min (200 μg mL^{-1}, 1.0 W cm^{-2}).

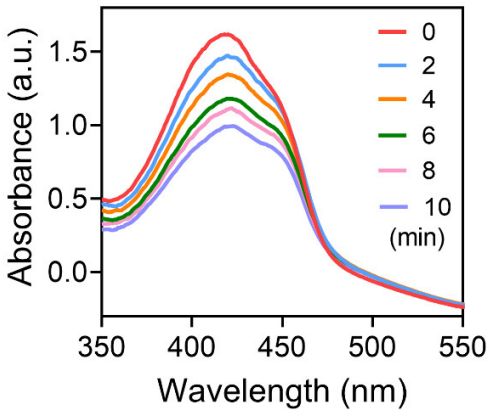

Fig. S20. UV-vis absorption spectra of DPBF containing TPAD-COF NPs solution under NIR laser irradiation for 10 min (200 μg mL^{-1}, 1.0 W cm^{-2}).

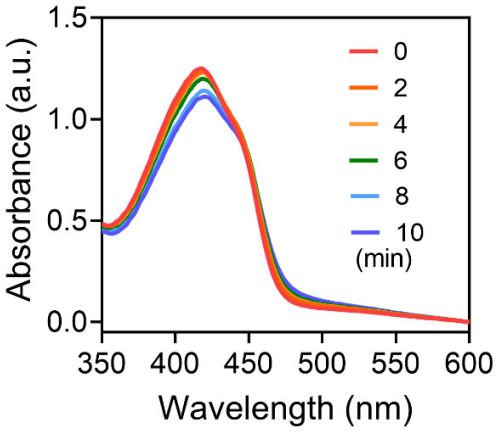

Fig. S21. UV-vis absorption spectra of DPBF containing TPAD-COF NPs for 10 min without NIR laser irradiation.

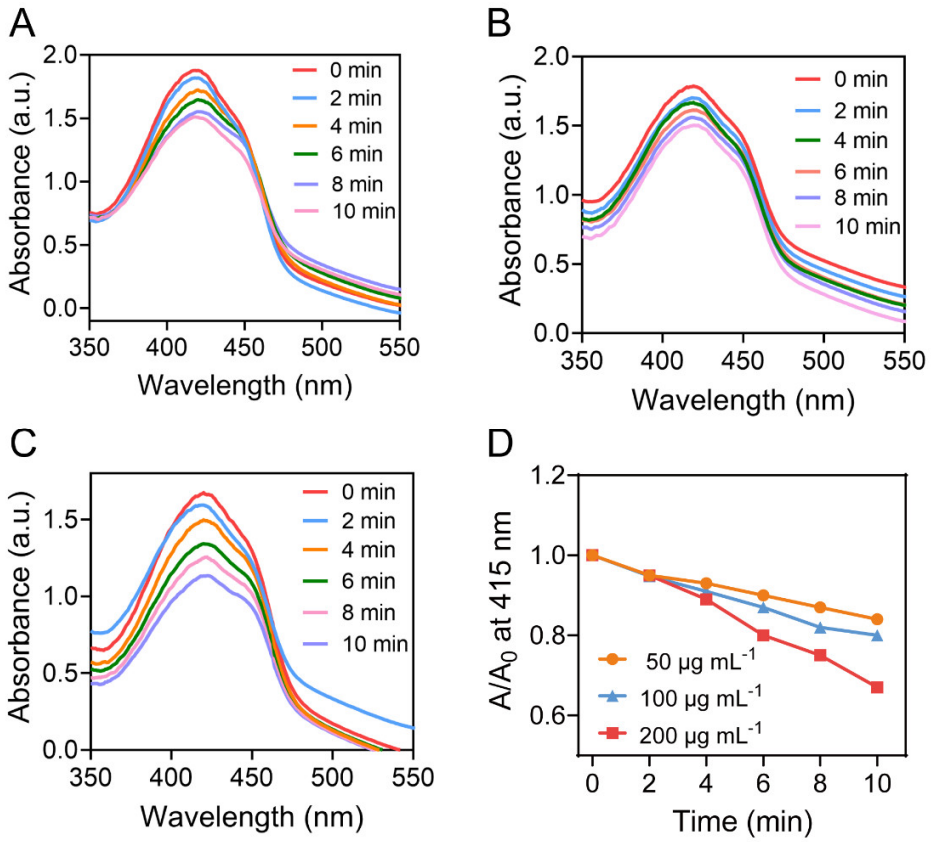

Fig. S22. UV-vis absorption spectra of DPBF solution containing TPAD-COF NPs at different doses, including (**A**) 50 μg mL^{-1}, (**B**) 100 μg mL^{-1}, (**C**) 200 μg mL^{-1}. (**D**) Normalized changes in the absorbance of DPBF solution at 415 nm at diverse concentrations.

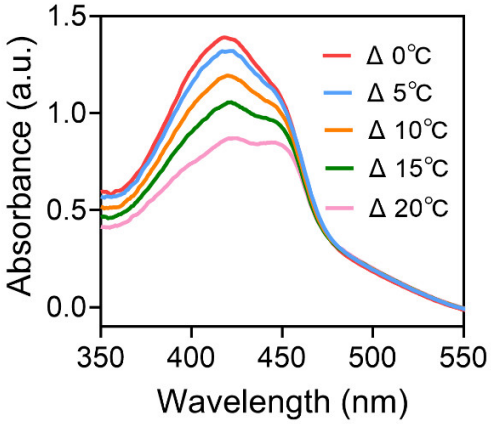

Fig. S23. UV-vis absorption spectra of DPBF solution containing TPAD-COF NPs under increasing temperature gradients (1.0 W cm^{-2}).

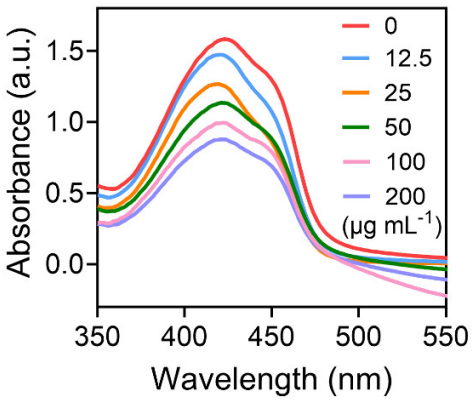

Fig. S24. UV-vis absorption spectra of DPBF solution containing elevating doses of TPAD-COF NPs under NIR laser irradiation (1.0 W cm^{-2}).

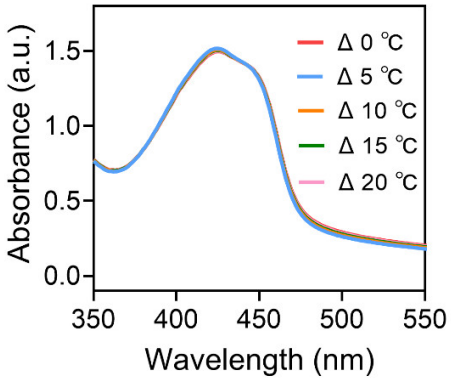

Fig. S25. UV-vis absorption spectra of DPBF solution alone at increasing temperature gradients.

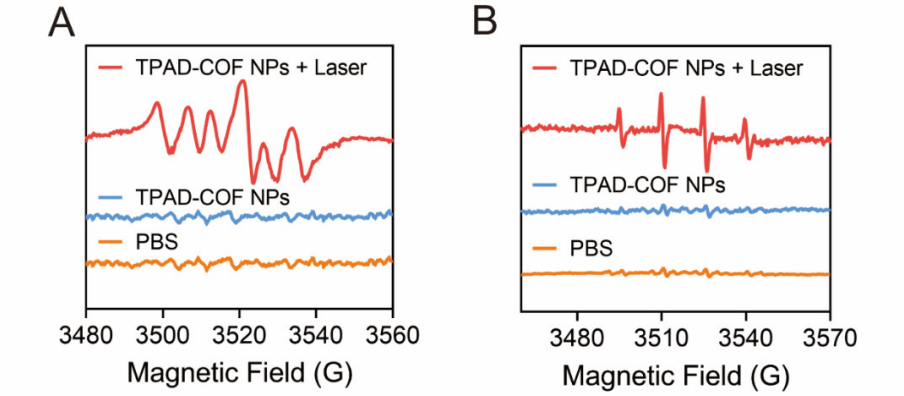

Fig. S26. ESR spectra illustrating (**A**) $\bullet O_2^-$ and (**B**) •OH generation in various treatment groups.

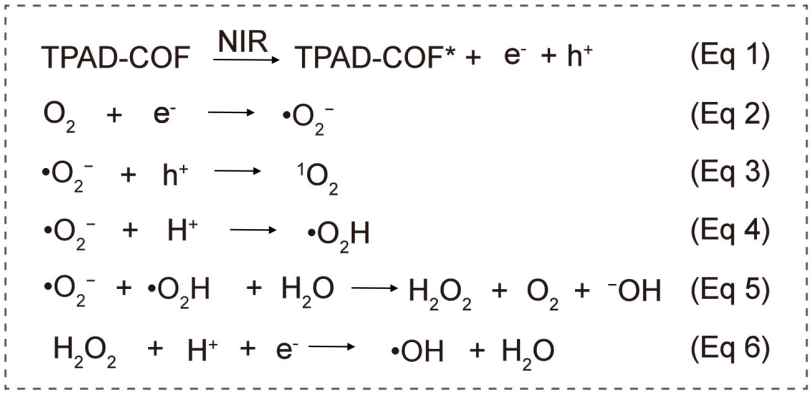

Fig. S27. The reaction steps for reactive oxygen species (ROS) generation.

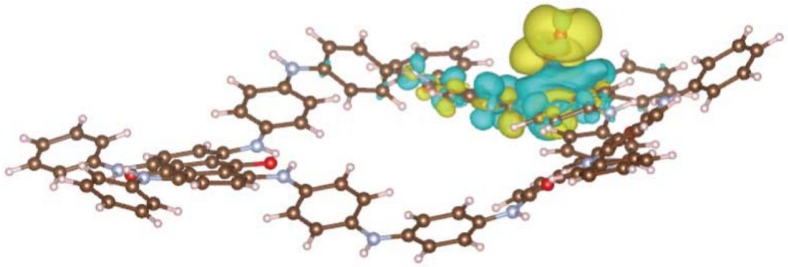

Fig. S28. Differential charge density plot of TPAD-COF NPs absorbed by O_2, with cyan and yellow indicating the regions of electron depletion and electron accumulation, respectively.

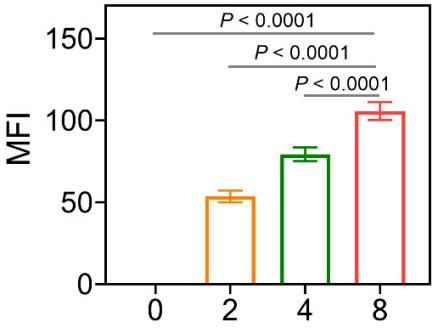

Fig. S29. Quantitative analysis of 4T1 cell uptake after incubation of Cy5.5-labeled TPAD-COF NPs for various durations by confocal laser scanning microscopy (CLSM) observation (n = 3). Data are represented as mean ± SD and analyzed by one-way ANOVA test.

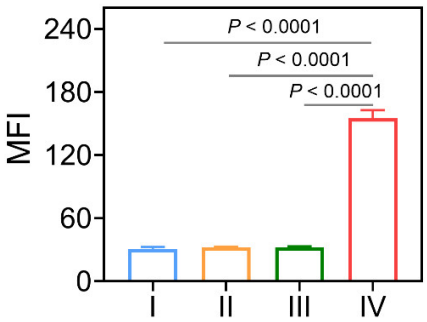

Fig. S30. Quantitative analysis of the fluorescence intensity of 2',7'-dichlorofluorescein (DCF) in different treatment groups by CLSM observation (n = 3). I: Control, II: Laser (1.5 W cm^{-2}, 10 min), III: TPAD-COF NPs (100 μg mL^{-1}), and IV: TPAD-COF NPs (100 μg mL^{-1}) + Laser (1.5 W cm^{-2}, 10 min). Data are represented as mean ± SD and analyzed by one-way ANOVA test.

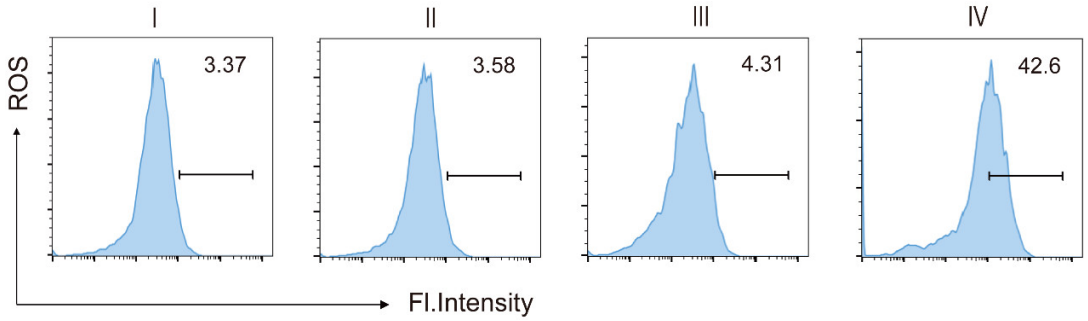

Fig. S31. Flow cytometry analysis of ROS generation in various treatment groups. I: Control, II: Laser (1 W cm^{-2}, 10 min), III: TPAD-COF NPs (100 μg mL^{-1}), and IV: TPAD-COF NPs (100 μg mL^{-1}) + Laser (1 W cm^{-2}, 10 min).

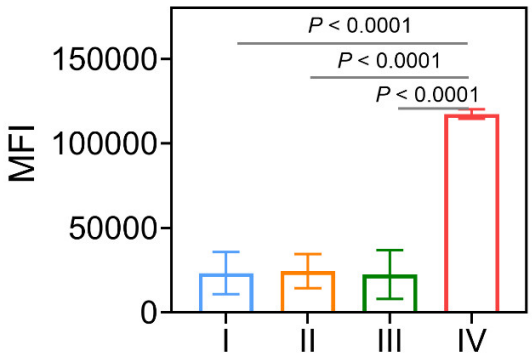

Fig. S32. Quantitative analysis of the mean fluorescence intensity of DCF after diverse treatments by flow cytometry analysis (n = 3). I: Control, II: Laser (1 W cm^{-2}, 10 min), III: TPAD-COF NPs (100 μg mL^{-1}), and IV: TPAD-COF NPs (100 μg mL^{-1}) + Laser (1 W cm^{-2}, 10 min). Data are represented as mean ± SD and analyzed by one-way ANOVA test.

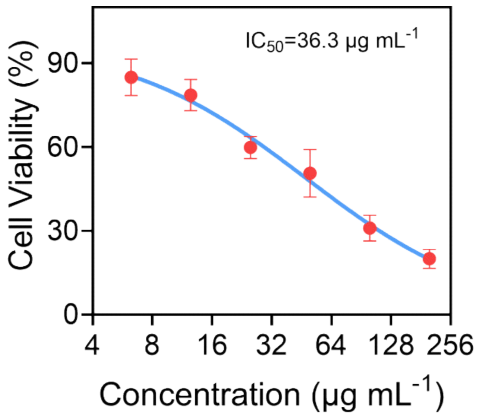

Fig. S33. The half maximal inhibitory concentration (IC_{50}) of TPAD-COF NPs under 808 nm laser irradiation for 10 min (n = 5). Data are represented as mean ± SD.

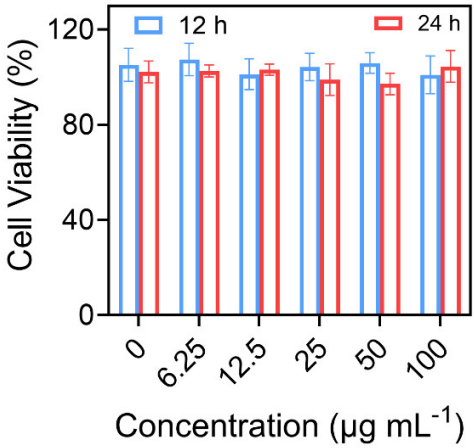

Fig. S34. Viability of HUVEC cells treated with various doses of TPAD-COF NPs for 12 and 24 h (n = 5). Data are represented as mean ± SD.

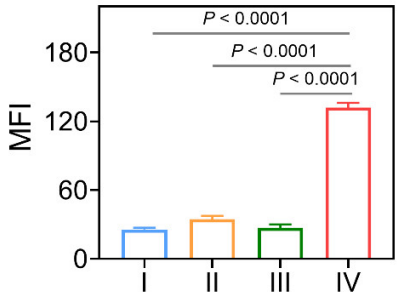

Fig. S35. Quantitative analysis of the mean fluorescence intensity of CRT after different treatments by CLSM (n = 3). I: Control, II: Laser (1 W cm^{-2}, 10 min), III: TPAD-COF NPs (100 μg mL^{-1}), and IV: TPAD-COF NPs (100 μg mL^{-1}) + Laser (1 W cm^{-2}, 10 min). Data are represented as mean ± SD and analyzed by one-way ANOVA test.

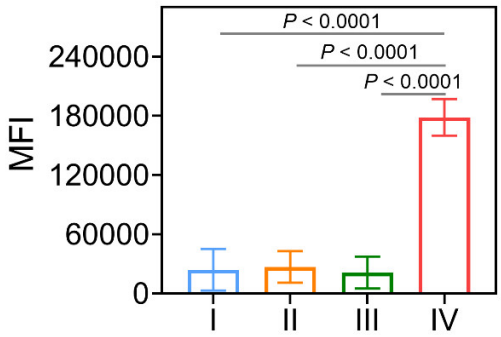

Fig. S36. Quantitative analysis of the mean fluorescence intensity of CRT after different treatments by flow cytometry analysis (n = 3). I: Control, II: Laser (1 W cm^{-2}, 10 min), III: TPAD-COF NPs (100 μg mL^{-1}), and IV: TPAD-COF NPs (100 μg mL^{-1}) + Laser (1 W cm^{-2}, 10 min). Data are represented as mean ± SD and analyzed by one-way ANOVA test.

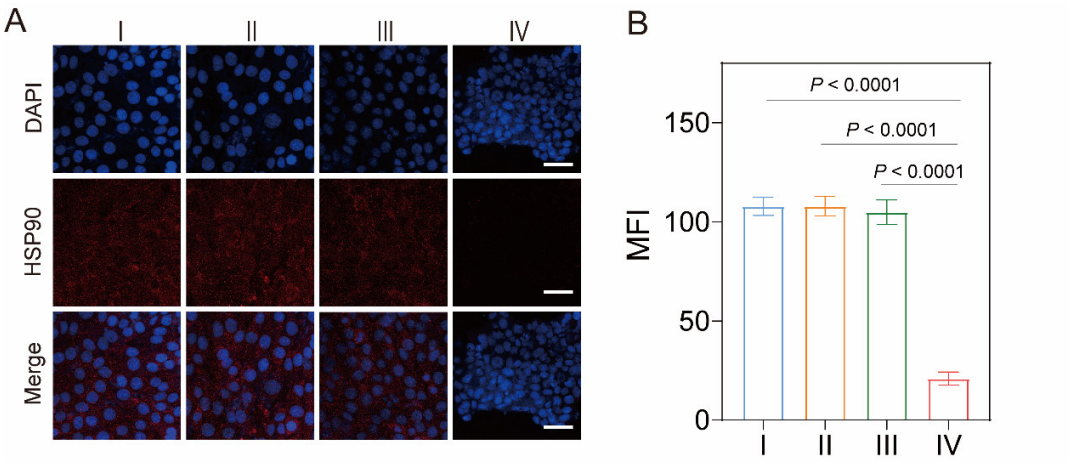

Fig. S37. (**A**) Immunofluorescence images of HSP90 expression in 4T1 cells from different treatment groups, and (**B**) the corresponding quantitative analysis of HSP90 fluorescence intensity (n = 3). I: Control, II: Laser (1 W cm^{-2}, 10 min), III: TPAD-COF NPs (100 μg mL^{-1}), and IV: TPAD-COF NPs (100 μg mL^{-1}) + Laser (1 W cm^{-2}, 10 min). Scale bar: 40 μm. Data are represented as mean ± SD and analyzed by one-way ANOVA test.

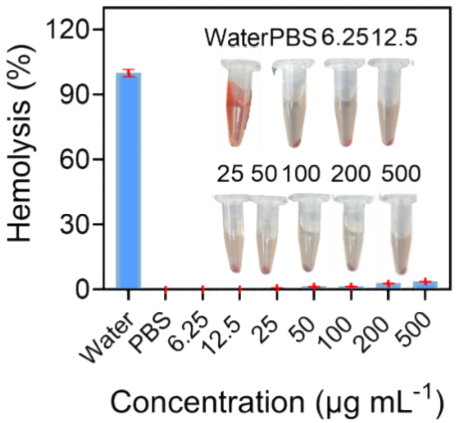

Fig. S38. Hemolytic activity of different concentrations of TPAD-COF NPs (n = 5). Inset: Photograph of blood supernatant containing different doses of TPAD-COF NPs.

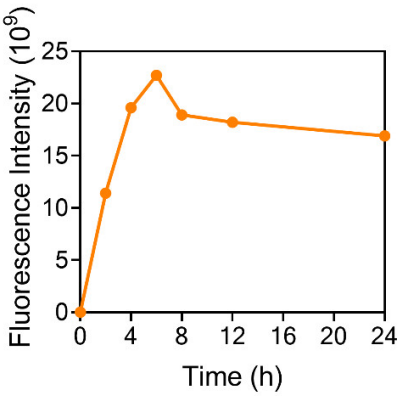

Fig. S39. Quantitative analysis of fluorescence intensity after intravenous injection of TPAD-COF NPs for various durations.

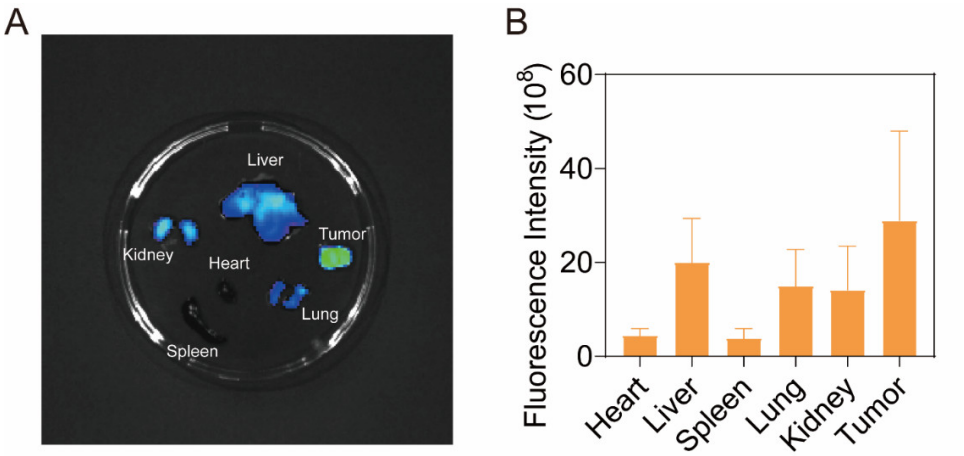

Fig. S40. (A) Fluorescence images, and (B) quantitative analysis of the main organs (heart, liver, spleen, lung, kidney) and tumor tissues of 4T1 tumor-bearing mice after intravenous injection (n = 3). Data are represented as mean ± SD.

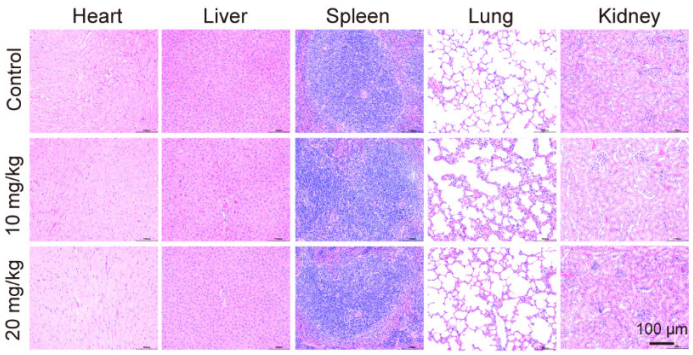

Fig. S41. H&E staining images of representative major organs from the mice after intravenous injection of different doses of TPAD-COF NPs for 15 days. Scale bar: 100 μm.

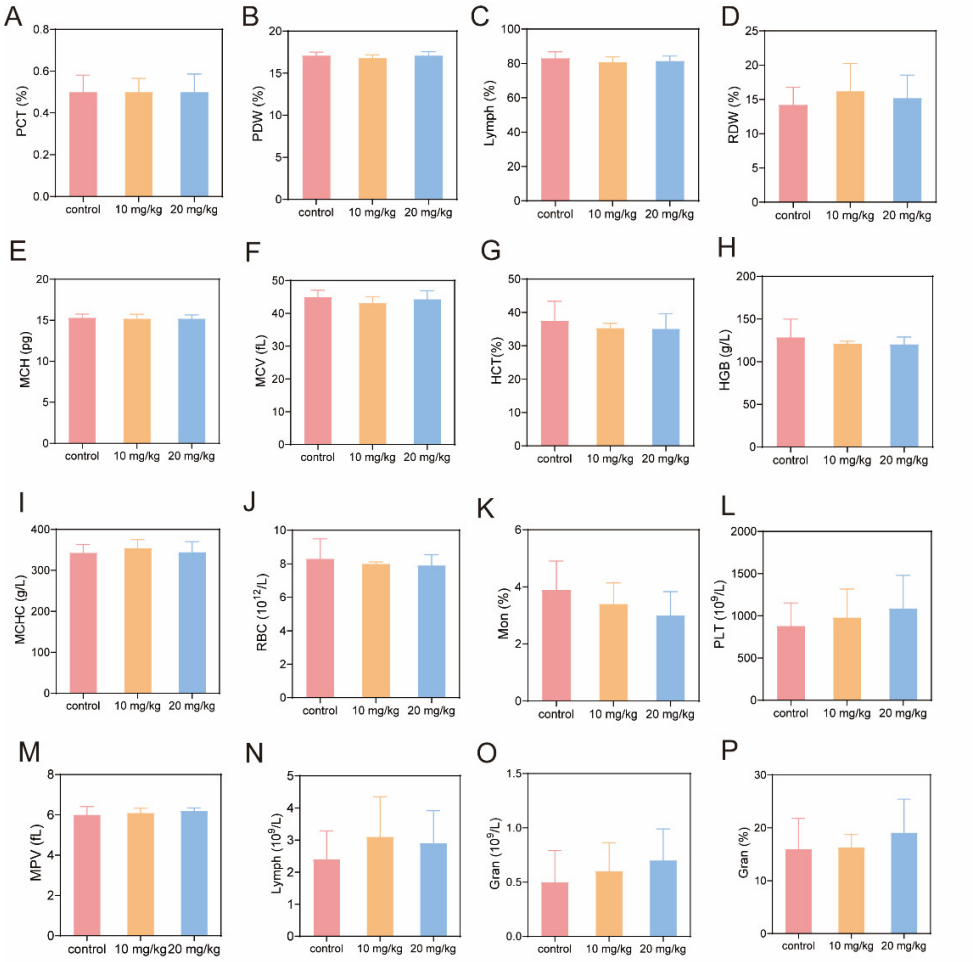

Fig. S42. Routine blood indexes of the Balb/c mice after intravenous injection with PBS (control) and different concentrations of TPAD-COF NPs, including (**A**) platelet distributing width (PCT), (**B**) platelet distribution width ratio (PDW%), (**C**) lymphocyte ratio (Lymph%), (**D**) red cell distribution width ratio (RDW%), (**E**) mean corpuscular hemoglobin (MCH), (**F**) mean corpuscular volume (MCV), (**G**) hematocrit ratio (HCT%), (**H**) hemoglobin (HGB), (**I**) mean corpuscular hemoglobin concentration (MCHC), (**J**) red blood cell (RBC), (**K**) absolute value of intermediate cell count ratio (Mon%), (**L**) platelet (PLT), (**M**) mean platelet volume (MPV), (**N**) lymphocytes (Lymph), (**O**) granulocyte (Gran), and (**P**) granulocyte ratio (Gran%) (n = 3).

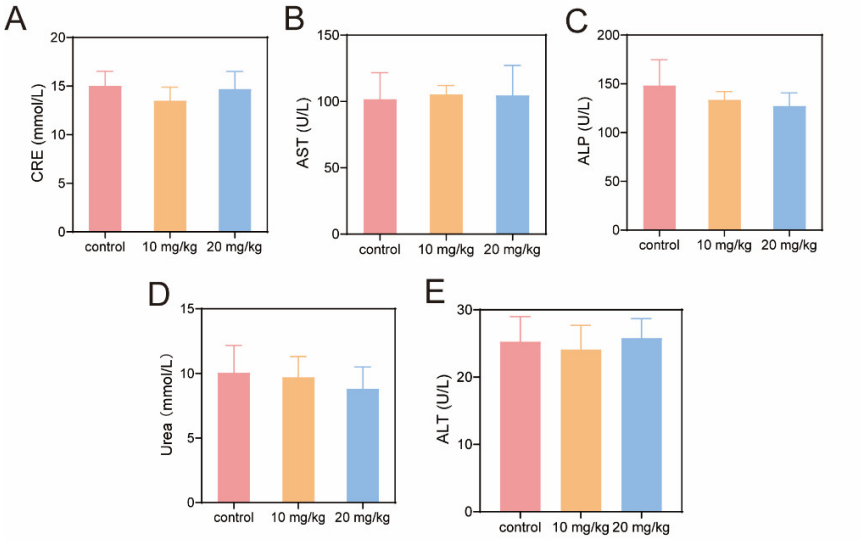

Fig. S43. Biochemical parameters of the Balb/c mice after intravenous injection with PBS (control) and diverse doses of TPAD-COF NPs, including (**A**) creatinine (CRE), (**B**) aspartate aminotransferase (AST), (**C**) alkaline phosphatase (ALP), (**D**) urea (Urea), and (**E**) alanine aminotransferase (ALT) (n = 3).

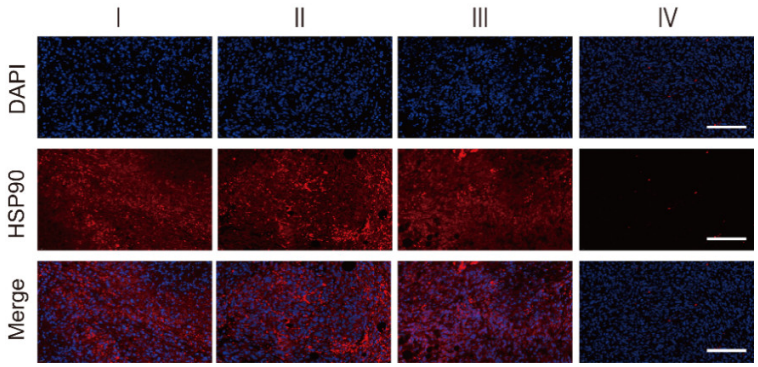

Fig. S44. Immunofluorescence images of HSP90 expression at tumor sites in different treatment groups. I: Control, II: Laser (1 W cm^{-2}, 10 min), III: TPAD-COF NPs (100 μg mL^{-1}), and IV: TPAD-COF NPs (100 μg mL^{-1}) + Laser (1 W cm^{-2}, 10 min). Scale bar: 100 μm.

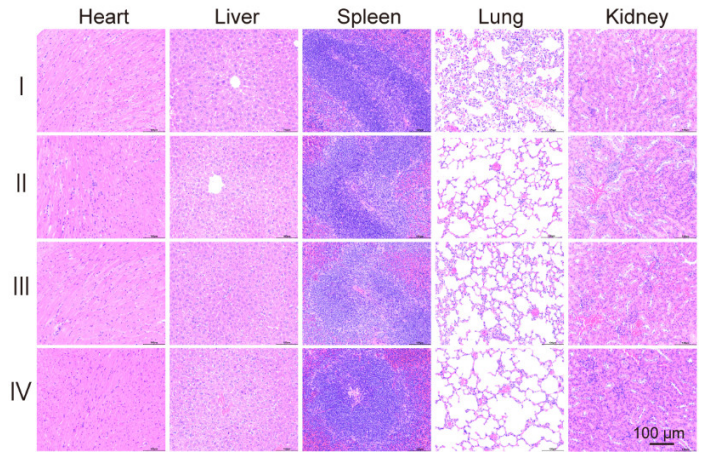

Fig. S45. H&E staining images of the major organs from the 4T1 tumor-bearing mice in various treatment groups. I: Control, II: Laser (1 W cm^{-2}, 10 min), III: TPAD-COF NPs (100 μg mL^{-1}), and IV: TPAD-COF NPs (100 μg mL^{-1}) + Laser (1 W cm^{-2}, 10 min). Scale bar: 100 μm.

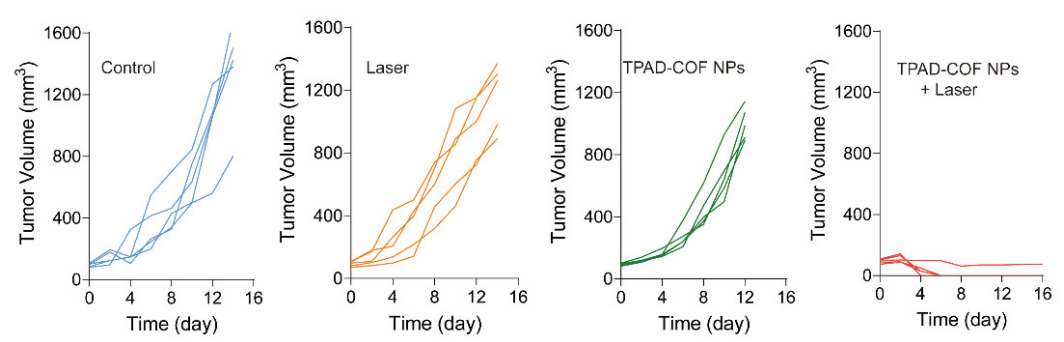

Fig. S46. Individual growth curves of primary tumors after different treatments (n = 5).

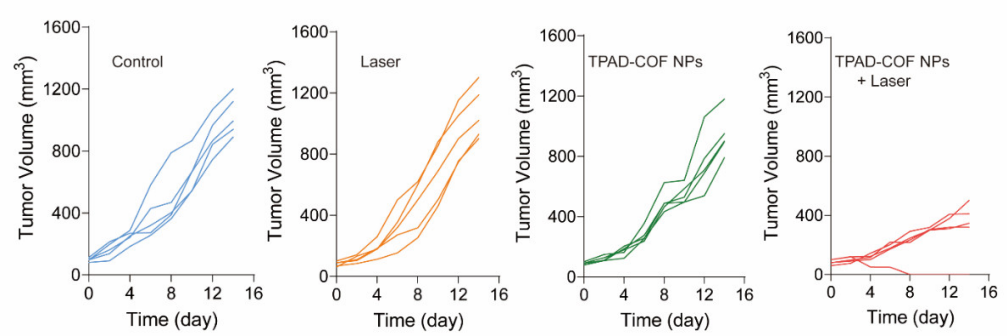

Fig. S47. Time-dependent growth curves of distant tumors after different treatments (n = 5).

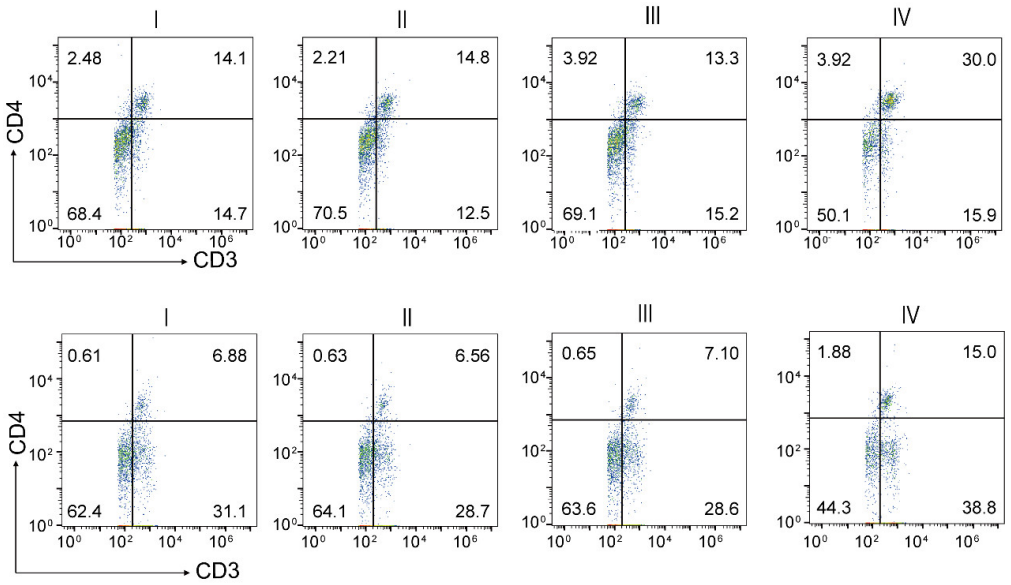

Fig. S48. Flow cytometry analysis of $CD3^+CD4^+$ and $CD3^+CD8^+$ T cells in tumor tissues of mice after different treatments. I: Control, II: Laser (1 W cm^{-2}, 10 min), III: TPAD-COF NPs (100 μg mL^{-1}), and IV: TPAD-COF NPs (100 μg mL^{-1}) + Laser (1 W cm^{-2}, 10 min).

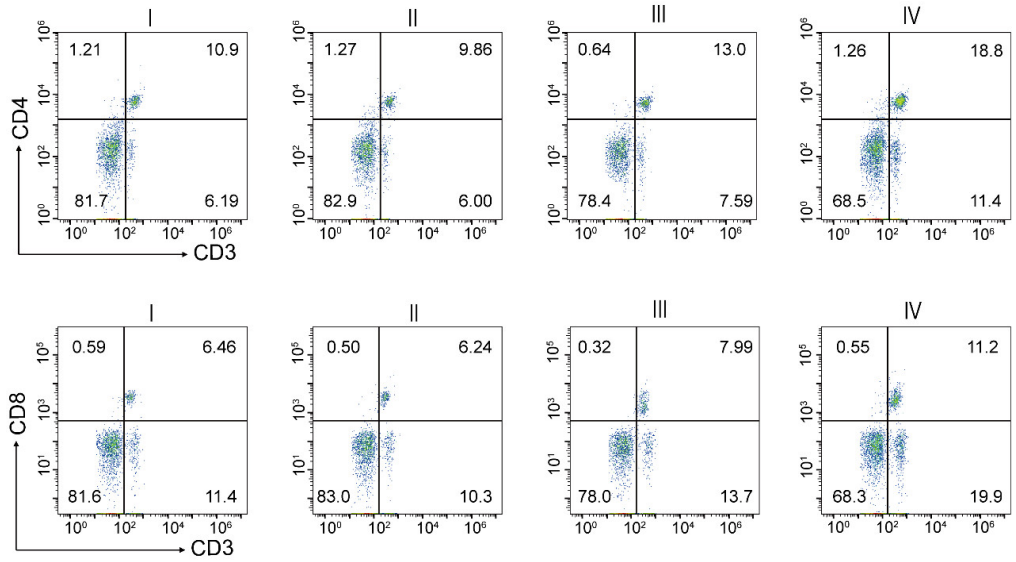

Fig. S49. Flow cytometry analysis of $CD3^+CD4^+$ and $CD3^+CD8^+$ T cells in spleen tissues of mice after different treatments. I: Control, II: Laser (1 W cm^{-2}, 10 min), III: TPAD-COF NPs (100 μg mL^{-1}), and IV: TPAD-COF NPs (100 μg mL^{-1}) + Laser (1 W cm^{-2}, 10 min).